Drift Capacity Modelling of Lightly Reinforced Concrete Columns

A. Wibowo[1], J.L. Wilson[1], N.T.K. Lam[2], E.F. Gad[1]

[1]Faculty of Engineering and Industrial Sciences, Swinburne University of Technology, Australia

[2]Department of Infrastructure Engineering, University of Melbourne, Australia

ABSTRACT:

Experimental laboratory testing of cast in-situ lightly reinforced concrete columns was conducted to investigate the collapse behaviour and drift capacity of such columns when subject to cyclic lateral loading. Four column specimens with a range of axial load and longitudinal reinforcement ratios were tested. The experimental results indicated that lightly reinforced concrete columns were able to sustain lateral drifts much greater than code and design guideline recommendations whilst maintaining axial load carrying capacity without catastrophic collapse.

Complementary theoretical analyses have been developed to model the lateral force-displacement relationship for the column by considering each of the flexural, yield penetration, and shear deformation displacement components. The theoretical model was shown to predict the experimental results with very good accuracy and could be used with confidence for further parametric studies involving other column configurations and axial loading scenarios.

KEYWORDS: drift capacity, axial load ratio, reinforced column tests, light reinforcement ratio, seismic performance

1. INTRODUCTION

An experimental laboratory test program has been developed to investigate the load-displacement and collapse mechanism behaviour of lightly reinforced concrete columns. Four column specimens were designed to represent a prototype of the non-ductile reinforced concrete columns of old buildings in low-to-moderate seismic regions as has been presented in Wibowo (AEES, 2010). The two parameters varied were the axial load and longitudinal steel reinforcement ratio. This paper presents the theoretical prediction developed to model force-deformation and drift capacity of such columns.

2. SPECIMEN DESIGN

Based on previous survey investigations (Rodsin, 2007; Wibowo, 2008, 2009a), it was shown that limited ductile columns can provide significant ductility capability despite a very low lateral load and drift capacity predicted from a conventional design perspective. Therefore, investigating the drift capability of such columns is the main objective of this research. Such limited ductile columns are characteristic of many older structures in developed countries and many new structures in developing countries, particularly in regions of low-to-moderate seismicity. Some of the characteristics of the columns include:

- Moderate aspect ratio in the range 2-4
- Longitudinal reinforcement steel ratio of 1%-2% or less.
- Limited lateral confinement reinforcement steel ratio of around 0.1%
- Axial load ratio in the range 0.1-0.4

The purpose of the present research project was to examine flexural-dominant and flexure-shear-dominant. The column specimens for the laboratory experimental tests were designed with the sectional properties similar to the existing precast soft-storey column (Wibowo, 2010a) whilst still maintaining the sectional properties within the range of specifications listed above. Details are presented in Table 1 and Figure 1, whilst the test setup is shown in Figure 2.

Table 1 Basic Properties of Column Specimens

Spec	Dimension (mm)	a (mm)	a/d	ρ_V	Main Rebars	ρ_H		Stirrups (@mm)	n	f_c' (MPa)	Hook type
						Area	Volumetric				
S1	270×300×1200	1200	4	0.56 %	4N12	0.08 %	0.10 %	R6@300	0.2	20.3	135°
S2	270×300×1200	1200	4	1.0 %	4N16	0.08 %	0.10 %	R6@300	0.2	21.0	135°
S3	270×300×1200	1200	4	1.0 %	4N16	0.08 %	0.10 %	R6@300	0.4	18.4	135°
S4	270×300×1200	1200	4	0.56 %	4N12	0.08 %	0.10 %	R6@300	0.4	23.7	135°

Notation : a is shear span which is the clear-height of the column in this case, *a/d* is the aspect ratio or shear span-to-depth ratio defined as shear span divided by the depth, *n* is the axial load ratio (ratio of the axial load to axial load-carrying capacity or $A_g f_c'$), ρ_V is the longitudinal reinforcement ratio ($\rho_V = A_s/A_g$), ρ_H is the lateral reinforcement (A_{sh}/bs), A_{sh} = total area of transverse reinforcement; s = tie spacing; and b = column section width.

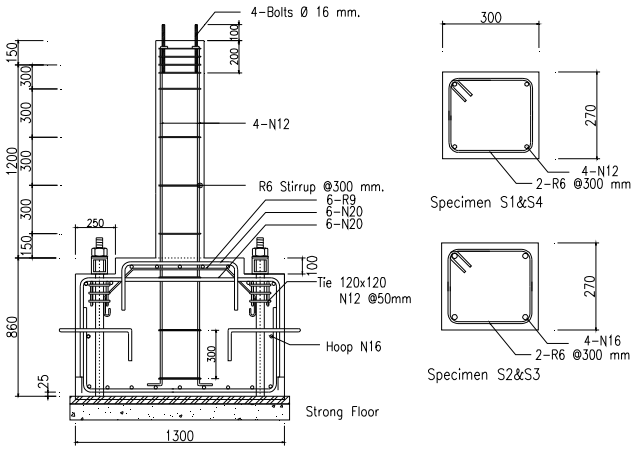

Figure 1 Geometry and reinforcement details of column specimens

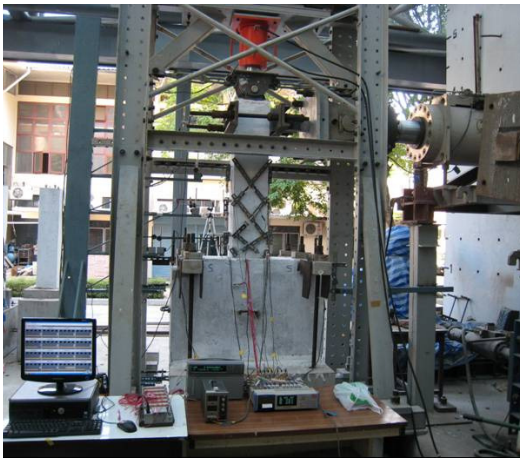

Figure 2 Experimental test setup

3. EXPERIMENTAL RESULTS

The hysteretic behaviour, drift component measurements (flexural, yield penetration, and shear displacements), together with the drift capacities from the experimental program have been presented in the previous AEES paper (Wibowo, 2010c). The summary of all column experimental results are presented in Table 2 and Figure 3, whilst the measurement of average curvature and shear deformation for each column regions are presented in subsequent sections.

The first crack and first yield drift values for specimens S1 and S2 were less than those of specimens S3 and S4. Conversely, the peak strength of specimens S1 and S2 occurred at larger drifts than those of specimens S3 and S4. This phenomenon might be attributed to the higher axial load ratio of specimens S3 and S4 that increased the compressive stress of column cross

sections, and in turn reduced the curvature ductility capacity through an increase of yield curvature and a decrease of ultimate curvature. Moreover, the effect of the axial load ratio to the drift capacity at axial failure showed that increasing the axial load ratio from 20% to 40% of concrete strength f'_cA_g resulted in a reduction of drift at axial failure. Further, the larger effect was found on columns with lower longitudinal reinforcement ratio. For example, drift at axial failure of specimen S1 reduced to about one third of that of specimen S4, both with longitudinal reinforcement ratio of 0.56%; whilst, the reduction was just about 50% for columns with longitudinal reinforcement ratio of 1.0%.

Table 2 Experimental results for specimens S1-S4

Parameters	Unit	S1	S2	S3	S4
V_{cr}	KN	23.7	28.4	34.5	38.6
V_y	KN	51.2	66.7	79.4	76.0
V_{max}	KN	59.7	78.4	82.9	77.0
$V_{80\%}$	KN	47.8	62.7	67.0	64.0
$V_{collapse}$	KN	18.4	28.3	67.0	64.0
δ_{cr}	% drift	0.13	0.13	0.20	0.20
δ_y	% drift	0.75	0.75	1.00	1.00
δ_{Vmax}	% drift	1.71	1.73	1.12	1.01
$\delta_{80\%}$	% drift	3.30	2.10	1.50	1.50
$\delta_{collapse}$	% drift	5.00	2.50	1.50	1.50

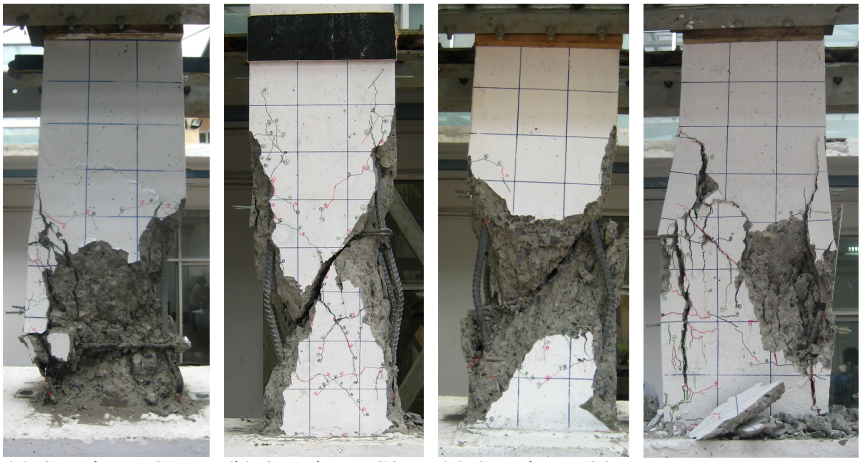

(a) Specimen S1 (b) Specimen S2 (c) Specimen S3 (d) Specimen S4

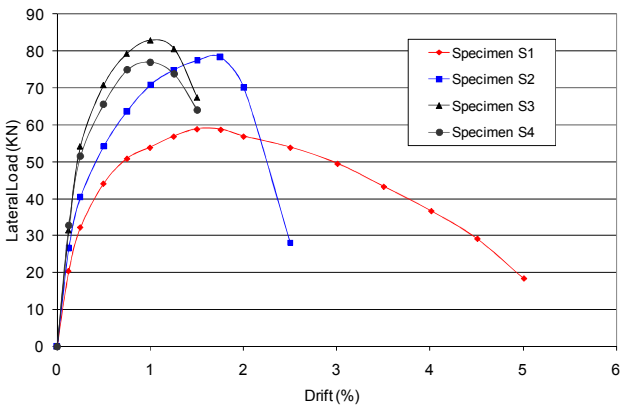

(e) The envelope curve of all specimens

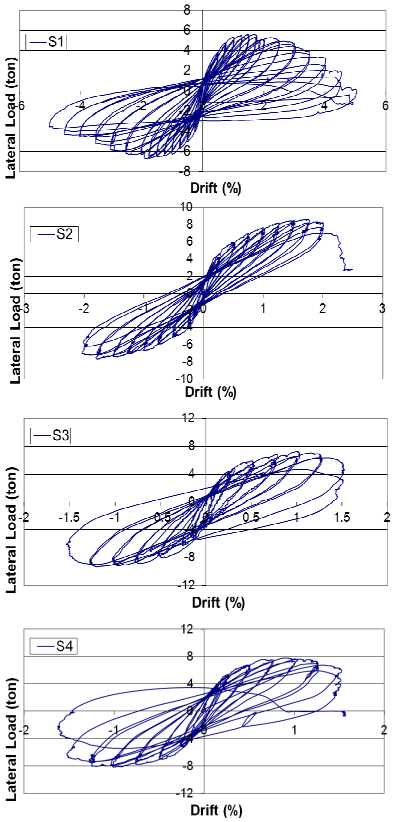

(f) Hysteresis Curve of each specimen

Figure 3 Results of Experiment Test (Wibowo, 2010c)

4. THEORETICAL DISPLACEMENT ANALYSIS

The lateral displacement of a column (Δ_{tot}) consists of three components, flexural (Δ_{fl}), yield penetration (Δ_{yp}) and shear deformation (Δ_{sh}) which are explained from an analytical perspective in this section.

$$\Delta_{tot} = \Delta_{fl} + \Delta_{yp} + \Delta_{sh} \quad (1)$$

4.1 Flexural Displacement

Flexural deflection prediction of the member is well understood and evaluated by performing curvature integration over the column height, where the curvature distribution is obtained commonly using a fibre section model. Additional plastic hinge analysis is needed to determine the inelastic deformation when curvatures at the maximum moment region exceed the yield value.

The average curvature has been calculated using Equation 2 over four segments up the height of the column as shown in Figure 4. The three lower segments which covered the predicted cracked region were instrumented with LVDTs, whilst the average curvature of the upper segment could be conservatively calculated using elastic principle since no cracks were observed in this region.

$$\varphi = \frac{\beta}{L_V} = \frac{\delta_{f2} - \delta_{f1}}{L_h} \cdot \frac{1}{L_V} \quad (2)$$

where L_v = height per each segment, L_h = distance between flexural LVDTs, δ_f = vertical LVDT measurement. Figure 4 presents the measured average curvature over the height of column. It can be observed that only specimen S1 developed a plastic hinge mechanism within the predicted plastic hinge length, whilst the plastic hinge region of the other three specimens S2, S3, and S4 extended to the second stirrup.

Using a tri-linear representation of the measured curvature distribution, the plastic hinge lengths for all specimens were estimated as shown in Table 4. Specimen S3 with the highest axial load ratio (n=0.4) and longitudinal reinforcement ratio (ρ_v=1.0%) had the largest plastic hinge region. Further, the longitudinal steel ratio had a greater effect on spreading the plastic hinge region compared with the axial force ratio (compare S1 and S2 when n=0.1 and S3 and S4 when n=0.4). The increase of axial load ratio from $0.2A_gf_c'$ to $0.4A_gf_c'$ increased the plastic hinge length in the order of 10%, whilst the increase of longitudinal reinforcement ratio from 0.56% to 1.0% increased the plastic hinge length of about 28%.

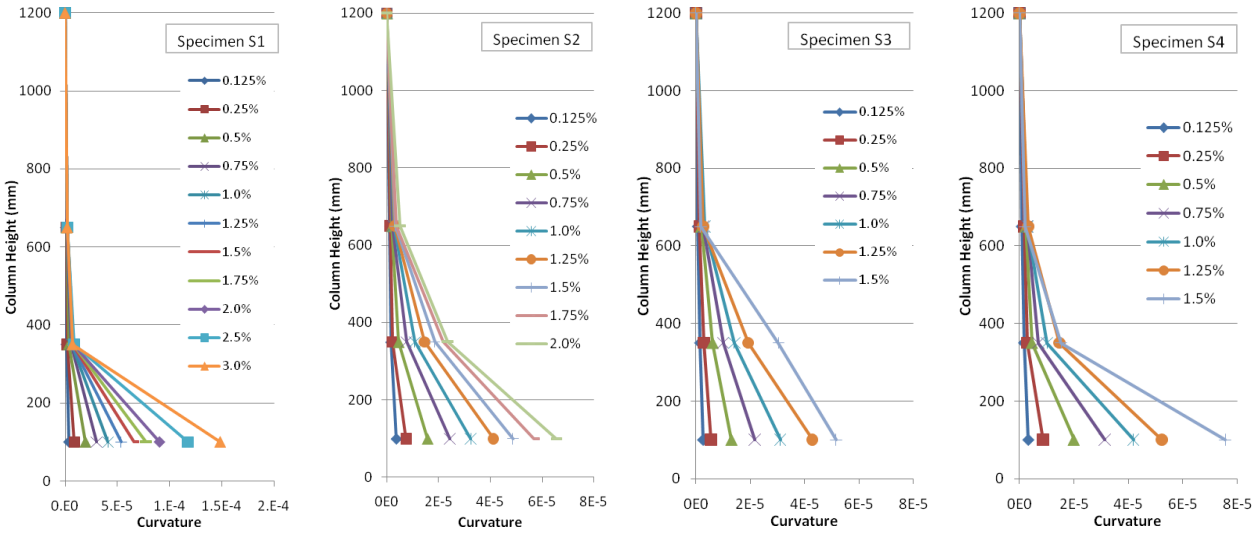

Figure 4 Curvature distributions over the column height of all specimens

There are numerous empirical models (Mattock 1967, Priestley 1996, Sawyer 1964, Park and Paulay 1975) that can be used to predict the equivalent plastic hinge length of ductile columns (refer Table 3) using the general equation as a function of shear span length, L, section width, D, and diameter of main bars, d_b, as follows:

$$L_p = \alpha L + \beta D + \xi f_y d_b \quad (3)$$

Where L is shear span length, D is effective depth of the section and d_b is diameter of longitudinal reinforcement

Table 3 Predicted and Measured Plastic Hinge Lengths

	α	β	ζ	L_p (mm)			
				S1	S2	S3	S4
Mattock, 1967	0.05	0.5	0	210	210	210	210
Priestley, 1996	0.08	0	0.022	238	285	285	238
Sawyer, 1964	0.075	0.25	0	165	165	165	165
Park and Paulay, 1975	0	0.5	0	132	133	133	132
Average Plastic Hinge Length (experimental)				170	220	240	190

For the design purpose of lightly reinforced concrete, the plastic hinge length could be conservatively assumed equal to the tie spacing, since the plastic hinge region is limited by the length of spalling concrete where the plastic rotation is mostly concentrated. It was observed from the tests that the concrete spalling was localised and was limited to the region where the bar buckling occurred which was approximately equal to the tie spacing. Therefore, the spacing of stirrups can be taken as an upper limit of plastic hinge length for lightly reinforced concrete columns. Whilst, for a lower bound, the Park and Paulay model provides a conservative estimate as shown in Table 4.

In this study, a computer program based on a fibre section analysis (Park and Paulay, 1975) has been developed to predict flexural deformation of the column, and the results are compared with the experimental outcomes as presented in Figure 5.

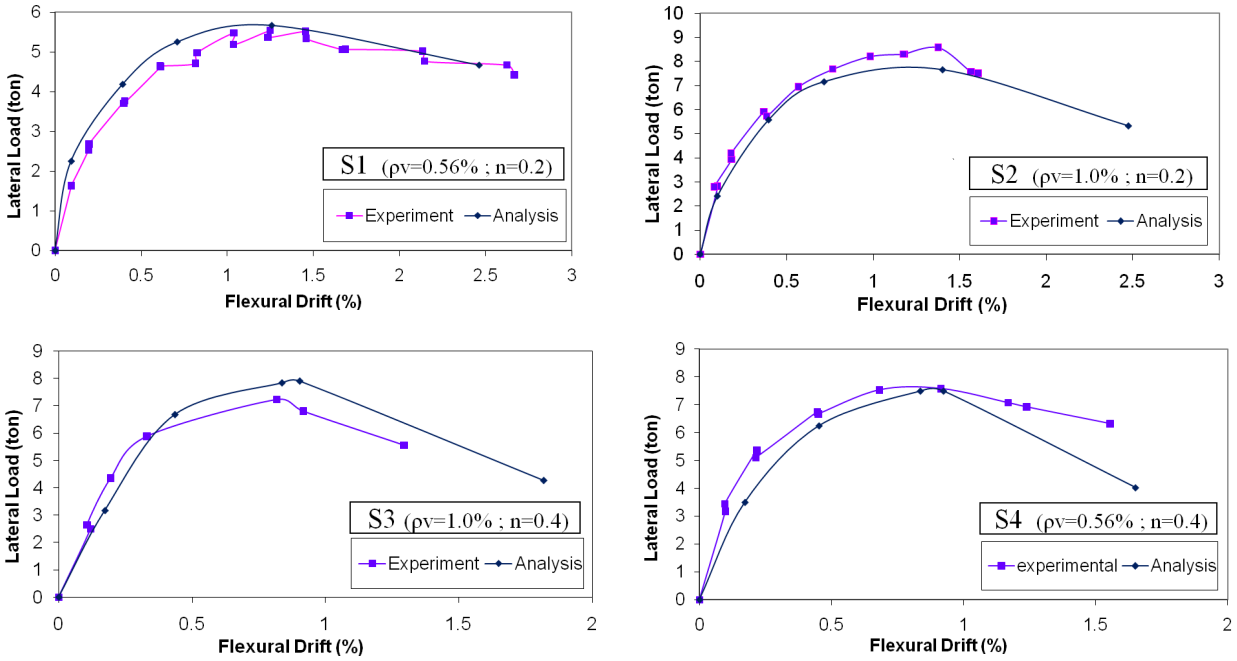

Figure 5 Comparison of flexural drift components between Experimental and Analytical results
(Note: each curve ends at the drift where the LVDTs were removed during experimental and not the drifts at axial failure.)

4.2 Yield penetration Displacement

Yield penetration behaviour has been widely investigated over the last two decades. A classical moment-curvature relationship has been used widely in calculating the slip gap opening by many previous researches. The main problem with these methods is that the steel stress and strain obtained at gap opening is based on strain compatibility between the steel and the concrete, whereas the presence of a gap opening at the column base prevents the use of closed form solution to predict the neutral axis depth because of strain incompatibility between the steel and concrete at the connection interface. A trial-and-error procedure is usually needed to evaluate the neutral axis depth through a convergence process of slip displacement, steel stress-strain, and yield penetration length. However, this approach is not suitable for design purposes of new columns, and to address this deficiency, this paper proposes a closed form model to predict the slip displacement and related parameters.

The proposed model and algorithm have been developed based on a displacement-controlled principle by proposing a new approach that uses the stress-strain relationship estimate and geometrical compatibility to solve the strain incompatibility between the steel and concrete (refer Figure 6). Further, a complete algorithm is presented by modifying the fibre cross section analysis to operate under curvature control as a function of the top column displacement instead of strain control as follows:

1. Fix increment of global displacement of Δ_{top}, and calculate the related rotation for each Δ_{top} increment.

$$\theta_{slip} = \theta = \frac{\Delta_{top}}{L} \tag{4}$$

2. Guess an initial value of concrete strain ε_c, and calculate neutral axis depth c from geometrical compatibility principle:
   a. Evaluate curvature, for each case :
      i. Strain compatibility *:* $\varphi = \frac{3\Delta_{top}}{L^2}$ (5)
      ii. Strain incompatibility : $\varphi = \frac{\Delta_{top}}{L}$ (6)
   b. Evaluate neutral axis depth : $c = \varepsilon_c \, \rho = \frac{\varepsilon_c}{\varphi}$ (7)
   c. Evaluate steel deformation at gap slip interface, $\Delta_{slip} = \theta_{slip}(d\text{-}c)$ (8)
   d. Evaluate tensile steel strain ε_s

$$\varepsilon_s = \sqrt{\frac{8\Delta_{slip}\sqrt{f_c'}}{E_s d_b}} - \varepsilon_{init} \qquad \text{for } \varepsilon_s < \varepsilon_y \tag{9}$$

$$\varepsilon_s = \sqrt{\Delta_{slip}\frac{4\sqrt{f_c'}}{\eta d_b} + \varepsilon_y^{\,2}\left(1 - \frac{E_s}{2\eta}\right)} - \varepsilon_{init} \qquad \text{for } \varepsilon_s > \varepsilon_y \tag{10}$$

   where:

   $\varepsilon_{init} = \frac{P}{BDE_c}$ = initial strain due to external axial load and member self-weight.

   The related stress f_s can then be obtained from the steel stress-strain relationship.
   e. Evaluate section equilibrium,

$$C_c - T_s + C_s = P \tag{11}$$

Where: C_c is determined using moment-curvature analysis
T_s and C_s can be obtained from steel stress-strain relationship.

3. Iterate Step 2 with new value of ε_c until equilibrium equation is satisfied, and then calculate moment capacity with the updated value of c and ε_c.

$$M = C_c \frac{c}{2} - T_s d_{ts} + C_s d_{cs} - \left[P\left(\frac{D}{2} - \Delta\right) + W\left(\frac{D-\Delta}{2}\right) \right] \tag{12}$$

4. Calculate lateral load

$$F_h = M/L \tag{13}$$

5. Repeat the whole process for the next increment of deflection Δ_{top}

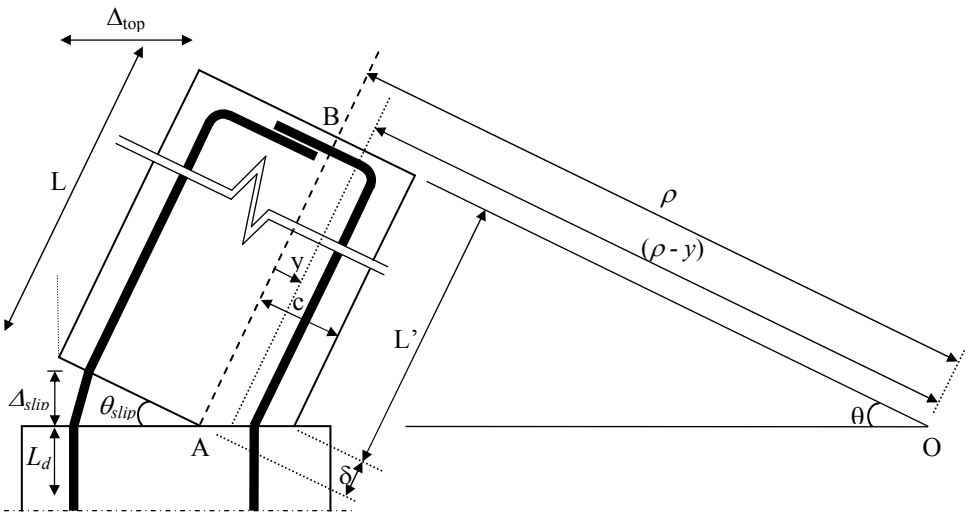

Figure 6 Gap opening mechanism for yield penetration analysis

The outcome of the proposed algorithm is the lateral load-displacement relationship for the yield penetration mechanism. For each value of lateral load obtained from the flexural calculation, the related displacement components of yield penetration can be determined as shown in Figure 7 for specimen S1. Good agreement between the experimental and analytical results for the lateral load versus yield penetration drift is demonstrated in Figure 8.

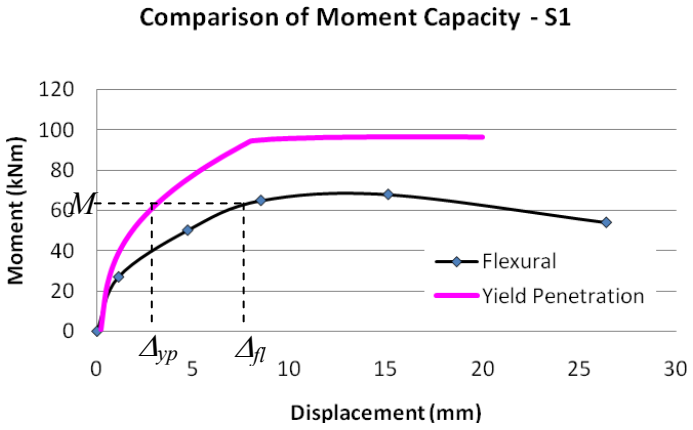

Figure 7 Moment-deflection relationship for the yield penetration components

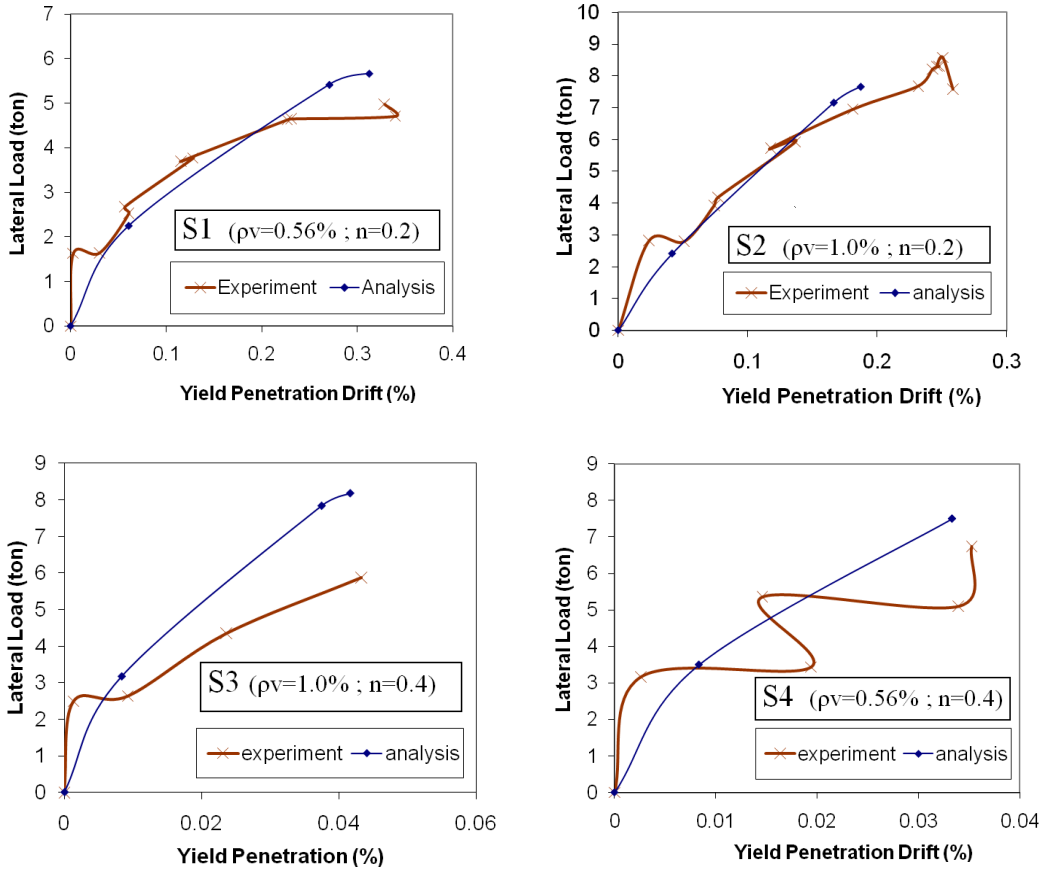

Figure 8 Comparison between experimental and analytical results for yield penetration drift

4.3 Shear Displacement

The average shear displacement over the height of the column was calculated using Equation 14 as follows:

$$\Delta_{sh} = \frac{(\delta_{s1} - \delta_{s2})}{2} \sec\xi = \frac{(\delta_{s1} - \delta_{s2})}{2} \frac{\sqrt{L_v{}^2 + D^2}}{L_v} \tag{14}$$

where δ_s = diagonal LVDT measurement, D = cross section depth (parallel to lateral loading direction) and is presented in Figure 9 for all specimens.

It was found that shear deformation of specimen S1 with the smallest longitudinal reinforcement ratio and axial load ratio was mostly concentrated in the plastic hinge region, whilst specimens S2, S3, and S4 developed shear deformation up to the second stirrup region. Prompt increase of shear deformation was observed in specimens S2, S3 and S4 that was attributed to rapid broadening and propagation of the main diagonal cracks. However, specimens S3 and S4 with higher axial load ratio developed larger shear deformation at an earlier stage of drift compared with specimen S2.

One more outcome observed is that shear deformation of specimen S3 (with the highest longitudinal steel ratio and axial load ratio) is distributed relatively equally over both the first and second stirrup regions, whilst shear deformation of specimen S2 and S4 was concentrated more in the region of the second stirrup.

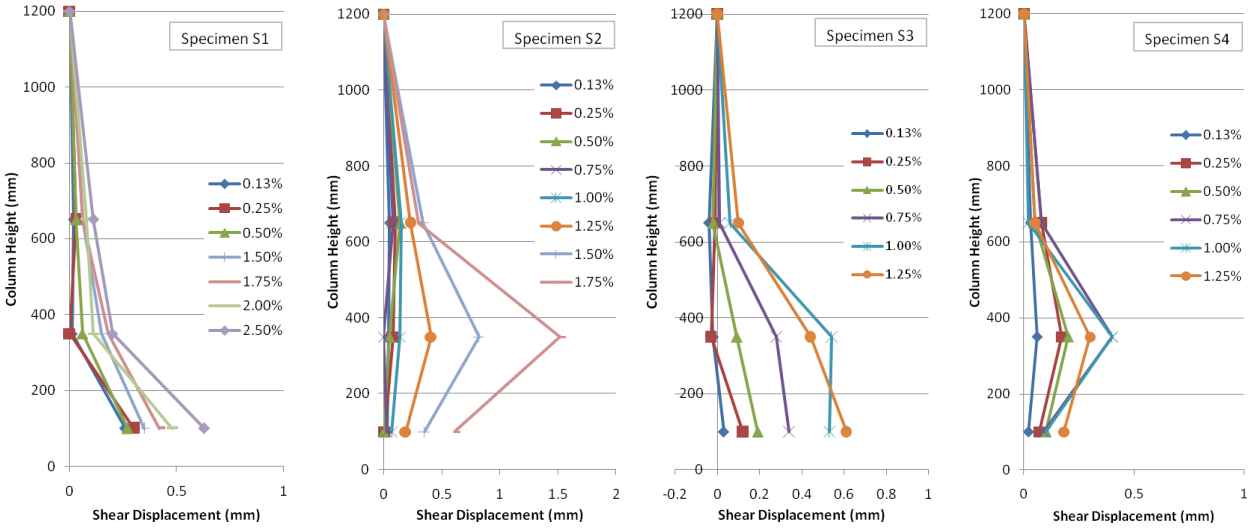

Figure 9 Shear displacement distributions over the column height of all specimens

An overview of the shear strength and shear deformation estimates is presented in the subsequent sections, but due to space limitations will not be described in detail in this paper.

4.3.1 Shear Strength Estimate

The proposed analytical method for assessing the shear strength has been developed based on the principal stress theory as suggested by Sezen (2002). The proposed shear strength model comprises contributions from the concrete (V_c) and transverse reinforcement (V_s) as follow:

$$V = (V_c + V_s) \tag{15}$$

$$V = \frac{2}{3} A_{cr} \sqrt{f_t^{\,2} + \frac{f_t P}{A_{cr}}} + \frac{A_{sv} f_{sy} d_o}{s} \tag{16}$$

Where

A_{cr} = cracked cross-sectional area of reinforced concrete column ($=0.85(n\rho_t)^{0.36} bd$)

f_t = the tensile concrete strength ($=0.4\sqrt{f'_c}$)

ρ_t = ratio of the cross-sectional area of longitudinal reinforcement in the tension zone to the effective concrete area ($=A_{st}/bd$).

4.3.2 Shear Deformation Estimate

For a limited ductile column, the contribution from shear deformation to total deformation is relatively small and hence the use of a complicated shear deformation model is not warranted. Further, since the openings of stirrups were barely found on any specimens, the elastic/service condition is reasonably assumed, and the shear deformation prediction by Park and Paulay (1975) can be used together with shear strength prediction by the proposed model. The developed shear deformation prediction consists of the uncracked and cracked regions. In this section, the results obtained from the model prediction were compared with the measured shear deformation from the test columns. The total shear deformation (δ_{sh}) can be calculated from the summation of the elastic shear deformation in the uncracked portion $\Delta_{vuncrack}$ and the shear deformation in the cracked portion Δ_{vcrack} as shown:

$$\Delta_{sh} = \Delta_{vuncrack} + \Delta_{vcrack} \tag{17}$$

A plot of predicted and measured shear deformation for all specimens is shown in Figure 10. The model predicted shear deformations with 40% axial load ratio (specimens S3 and S4) in good agreement with experimental results and reasonable agreement for specimens with 20% axial load ratio (S1 and S4). But overall, since the proportion of shear deformation to total deformation is very small for flexure dominant columns as shown in Figure 11, the predicted results are considered reasonable and satisfactory.

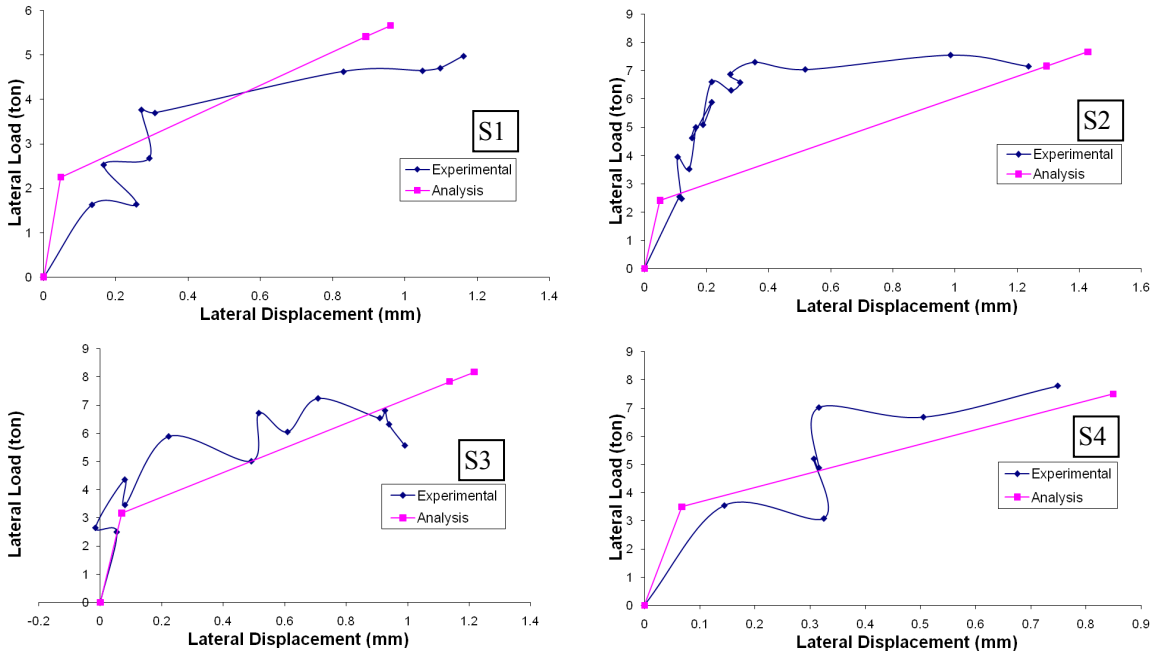

Figure 10 Shear displacement of all specimens.

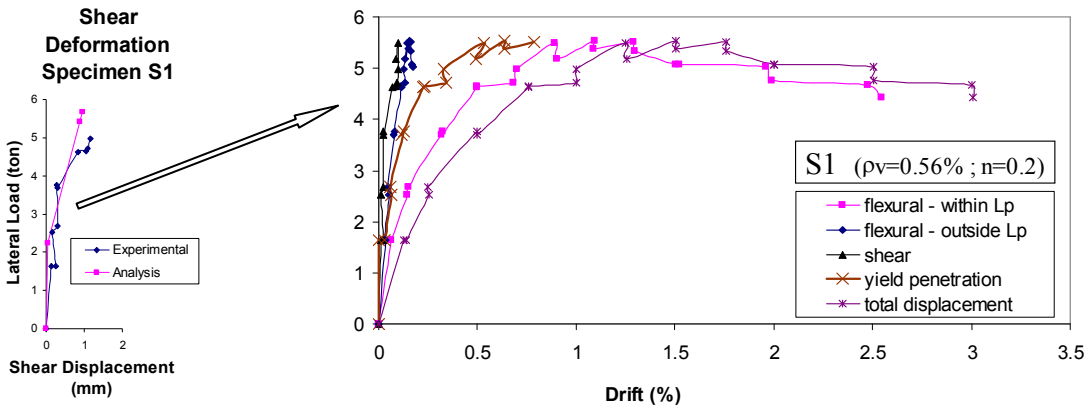

Figure 11 Contribution of shear to total drift

4.4 Total Lateral Displacement

The total displacement as a summation of the three components is shown in Table 4. The proposed model was used to construct the backbone force-drift curve which showed good agreement with the experimental hysteresis curves as shown in Figure 12.

Table 4 Total Drift

Results	Parameters	S1	S2	S3	S4	Stage
Theoretical Prediction	Displacement Δ_{top} (mm)	1.89	1.74	2.24	2.23	Crack
		12.64	11.89	11.62	11.28	Yield
		19.80	20.49	12.48	12.34	Ultimate
	Drift δ_{top} (%)	0.16	0.15	0.19	0.19	Crack
		0.85	0.89	0.97	0.94	Yield
		1.65	1.71	1.04	1.03	Ultimate
Experimental	Drift δ_{top} (%)	0.13	0.13	0.2	0.2	Crack
		0.75	0.75	1.0	1.0	Yield
		1.71	1.73	1.12	1.01	Ultimate

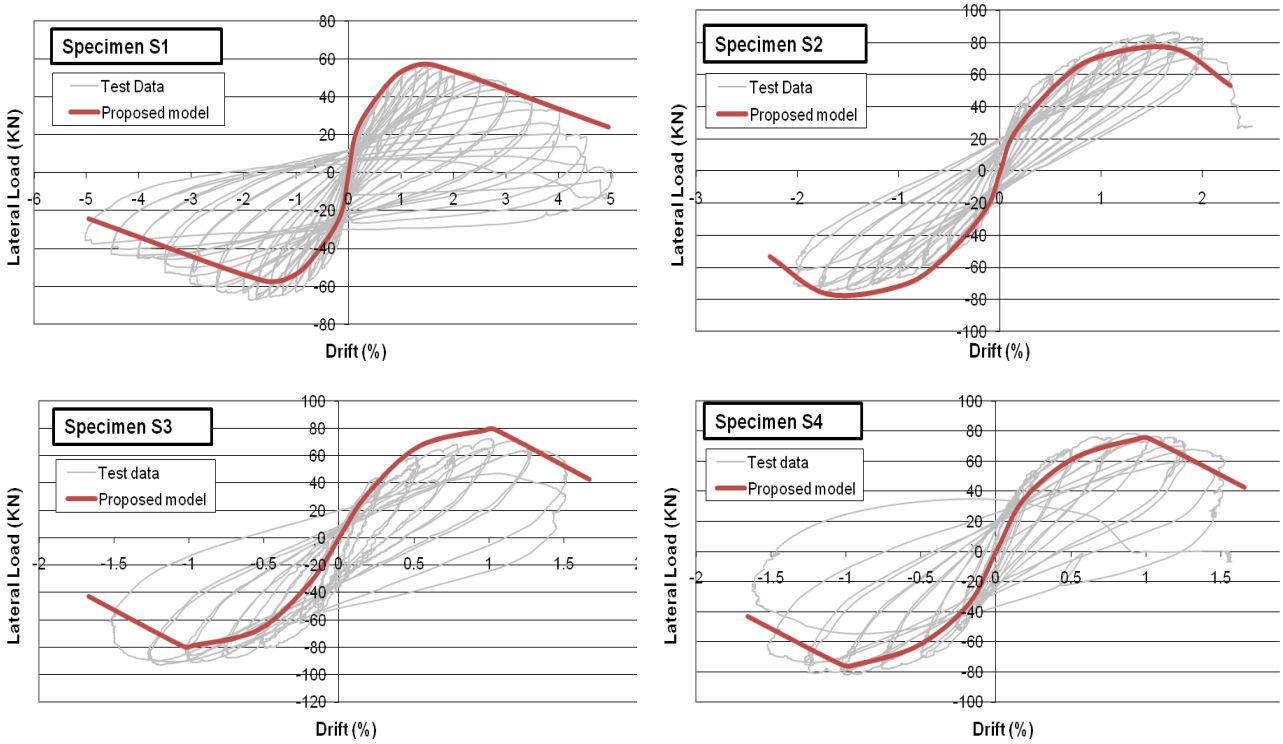

Figure 12 Experimental hysteretic curves versus the proposed model of backbone curve

5. CONCLUSION

Experimental research on four lightly reinforced concrete columns with axial load ratios n=0.2-0.4, longitudinal reinforcement ratio 0.56%-1.0% and transverse reinforcement ratio of 0.08% which was significantly less than minimum code requirement has been undertaken. The drift at axial load failure was at least 1.5% for all specimens despite the poor detailing and significantly greater than that predicted by current guidelines. In addition, the flexure, yield penetration and shear drift components and their effect on the overall behaviour have been presented in the paper.

REFERENCES

Park, R., Paulay, T. 1975. Reinforced Concrete Structures. *John Wiley & Sons*, New York. 769 pp.

Rodsin, K., 2007, Seismic Performance of Reinforced Concrete Soft-storey Buildings in Low to Moderate Seismicity Regions, *Ph.D. Dissertation*, Department of Civil and Environmental Engineering, University of Melbourne, Melbourne.

Sezen, H., 2002, Seismic Response and Modeling of Reinforced Concrete Building Columns, *Ph.D. Dissertation*, Department of Civil and Environmental Engineering, University of California, Berkeley.

Sezen, H., and Moehle, JP, 2003. Bond-slip behavior of reinforced concrete members, *fib-Symposium: Concrete Structures in Seismic Regions*, CEB-FIP, Athens, Greece. 2004.

Sezen, H. and Moehle, J.P. 2004. Shear strength model for lightly reinforced concrete columns. *Journal of Structural Engineering*, ASCE, Vol. 130(11), pp. 1692-1703.

Wibowo, A., Kafle, B., Kermani, A.M., Lam, N.T.K, Wilson, J.L., Gad, E.F. 2008. Damage in the 2008 China Earthquake. *Procs. of Australian Earthquake Engineering Society Conference*, Ballarat, Australia, 21-23 November.

Wibowo A, Wilson JL, Lam NTK, Gad EF. 2009a. "Modelling Precast Reinforced Concrete Columns and Comparisons with Results from Field Testings". *Procs. of The 1st International Conference on Computational Technologies in Concrete Structures (CTCS'09)*, Jeju, South Korea; 2009, 24-27 May, pp 184.

Wibowo A, Wilson JL, Gad EF., Lam NTK, Collier P. 2009 b. "Collapse Modelling Analysis of a Precast Soft-Storey Building in Melbourne". *Procs. of Australian Earthquake Engineering Society Conference*; Newcastle, New South Wales, Autralia, 2009, 11-13 Desember.

Wibowo A, Wilson JL, Gad EF, and Lam NTK. 2010a. Collapse Modelling Analysis of a Precast Soft-Storey Building in Melbourne. *Journal of Engineering Structure, Elsevier*. Special Issue: Learning Structural Failures, Vol. 32(7), July, pp 1925-1936.

Wibowo A, Wilson, J., Lam, N., Gad, EF. 2010b. "Drift Capacity of Precast Soft Storey Building in Melbourne". *Australian Journal of Structural Engineering*, Vol. 11(3), March, pp 177-194.

Wibowo A, Wilson JL, Lam NTK, Gad EF, Fardipour M, Rodsin K, Lukkunaprasit P, 2010c. "Drift Capacity of Lightly Reinforced Concrete". *Procs. of Australian Earthquake Engineering Society Conference*; Perth, Australia, 26-28 November, paper no.51.